nature COMMUNICATIONS

ARTICLE

Received 12 Jan 2014 | Accepted 21 Oct 2014 | Published 8 Jan 2015

DOI: 10.1038/ncomms6614

Mutations in *PNPLA6* are linked to photoreceptor degeneration and various forms of childhood blindness

S. Kmoch[1,*], J. Majewski[2,*], V. Ramamurthy[3,*], S. Cao[4,5], S. Fahiminiya[2], H. Ren[4,5], I.M. MacDonald[6], I. Lopez[4,5], V. Sun[4,5], V. Keser[4,5], A. Khan[4,5], V. Stránecký[1], H. Hartmannová[1], A. Přistoupilová[1], K. Hodaňová[1], L. Piherová[1], L. Kuchař[1], A. Baxová[7], R. Chen[8], O.G.P. Barsottini[9], A. Pyle[10], H. Griffin[10], M. Splitt[10], J. Sallum[11], J.L. Tolmie[12], J.R. Sampson[13], P. Chinnery[10], Care4Rare Canada[‡], E. Banin[14], D. Sharon[14], S. Dutta[15], R. Grebler[16], C. Helfrich-Foerster[16], J.L. Pedroso[9], D. Kretzschmar[15], M. Cayouette[3,17,18] & R.K. Koenekoop[4,5]

Blindness due to retinal degeneration affects millions of people worldwide, but many disease-causing mutations remain unknown. *PNPLA6* encodes the patatin-like phospholipase domain containing protein 6, also known as neuropathy target esterase (NTE), which is the target of toxic organophosphates that induce human paralysis due to severe axonopathy of large neurons. Mutations in *PNPLA6* also cause human spastic paraplegia characterized by motor neuron degeneration. Here we identify *PNPLA6* mutations in childhood blindness in seven families with retinal degeneration, including Leber congenital amaurosis and Oliver McFarlane syndrome. PNPLA6 localizes mostly at the inner segment plasma membrane in photoreceptors and mutations in *Drosophila PNPLA6* lead to photoreceptor cell death. We also report that lysophosphatidylcholine and lysophosphatidic acid levels are elevated in mutant *Drosophila*. These findings show a role for *PNPLA6* in photoreceptor survival and identify phospholipid metabolism as a potential therapeutic target for some forms of blindness.

[1] First Faculty of Medicine, Institute for Inherited Metabolic Disorders, Charles University in Prague, 120 00 Prague 2, Czech Republic. [2] Faculty of Medicine, Department of Human Genetics, McGill University and Genome Quebec Innovation Center, Montreal, Quebec, Canada H3A 0G1. [3] Cellular Neurobiology Research Unit, Institut de recherches cliniques de Montréal (IRCM), 110, Ave des Pins Ouest, Montreal, Quebec, Canada H2W 1R7. [4] McGill University, 845 Sherbrooke Street West, Montreal, Quebec, Canada H3A 0G4. [5] McGill Ocular Genetics Laboratory; Departments of Paediatric Surgery, Human Genetics and Ophthalmology, Montreal Children's Hospital, McGill University Health Centre, 2300 Tupper, Montreal, Quebec, Canada H3H 1P3. [6] Department of Ophthalmology and Visual Sciences, University of Alberta/Royal Alexandra Hospital, 10240 Kingsway Avenue, Edmonton, Alberta, Canada AB T5H 3V9. [7] First Faculty of Medicine, Institute of Biology and Medical Genetics, Charles University in Prague, 120 00 Prague 2, Czech Republic. [8] Human Genome Sequencing Center, Department of Molecular and Human Genetics, Baylor College of Medicine, One Baylor Plaza, Houston, Texas 77030, USA. [9] Division of General Neurology and Ataxia Unit, Department of Neurology, Universidade Federal de São Paulo, Sao Paulo 04021-001, Brazil. [10] Institute of Genetic Medicine, Newcastle University, Newcastle upon Tyne NE1 3BZ, UK. [11] Department of Ophthalmology, Universidade Federal de São Paulo, Sao Paulo 04021-001, Brazil. [12] Department of Clinical Genetics, Southern General Hospital, Glasgow G51 4TF, UK. [13] Institute of Medical Genetics, Cardiff University School of Medicine, Cardiff CF14 4XN, UK. [14] Department of Ophthalmology, Hadassah-Hebrew University Medical Center, Jerusalem 91120, Israel. [15] Oregon Institute of Occupational Health Sciences, Oregon Health and Science University, Portland, Oregon 97239, USA. [16] Lehrstuhl fuer Neurobiology und Genetik, Universitaet Wuerzburg, 97074 Wuerzburg, Germany. [17] Departement de Médecine, Université de Montréal, Montreal, Quebec, Canada H3T 1P1. [18] Division of Experimental Medicine, Department of Anatomy and Cell Biology, McGill University, Montreal, Quebec, Canada H3A 2B2. * Co-first authors. Correspondence and requests for materials should be addressed to D.K. (email: kretzsch@ohsu.edu) or to M.C. (email: michel.cayouette@ircm.qc.ca) or to R.K.K. (email: robert.koenekoop@mcgill.ca).
[‡] A list of authors and affiliations appears at the end of the paper.

PNPLA6 (also previously referred to as neuropathy target esterase (NTE)) is a highly conserved lysophospholipase anchored to the cytoplasmic face of the endoplasmic reticulum (ER)[1–3]. It is the primary target of toxic organophosphorous compounds (found in agricultural pesticides and agents of chemical warfare) that cause axonal degeneration in large neurons. Human organophosphorous-induced delayed neuropathy (OPIDN) occurs when PNPLA6 becomes phosphorylated by these organophosphates, followed by dealkylation of the phosphoryl enzyme, inhibiting the catalytic domain[4,5]. Patients with mutations in the catalytic domain of *PNPLA6* develop a Mendelian motor neuron disease called spastic paraplegia (SPG39), which is characterized by distal degeneration of motor axons surprisingly similar to OPIDN[6,7]. The exact mechanism of PNPLA6 function in both OPIDN and SPG39 remains unknown[8].

PNPLA6 is expressed in the brain, where it deacetylates phosphatidylcholine (PC) to lysophosphatidylcholine (LPC) and LPC to glycerophosphocholine[1,9]. In *Drosophila*, the Swiss cheese protein (sws; the orthologue of vertebrate PNPLA6) is involved in the regulation of membrane lipid homeostasis and in the survival of both neurons and glia as well[10]. In mice, *Pnpla6*-deficient animals are embryonic lethal[11] but brain-specific mutants show neurodegeneration[12], and there is much evidence that PNPLA6 is involved in maintaining nervous system integrity[13,14]. Interestingly, mice expressing a single copy of *Pnpla6* are viable but show increased sensitivity to organophosphorous toxins[11].

In this work, we identified biallelic *PNLPA6* mutations in patients with childhood blindness due to severe photoreceptor death and clinical features of Leber congenital amaurosis (LCA) and, interestingly, also of the rare Oliver McFarlane syndrome (OMS; OMIM 275400). OMS patients have a complex phenotype characterized by blindness due to severe photoreceptor degeneration, dwarfism due to pituitary growth hormone deficiency, trichomegaly and progressive alopecia. Occasionally, OMS is associated with mental retardation, distal muscle weakness/wasting and ataxia, due to axonal peripheral neuropathy. We document PNPLA6 expression in mouse and *Drosophila* retina, and test phenotypic and metabolic consequences (phospholipids) of *PNLPA6* and *SWS* mutations in humans and *Drosophila*, respectively. We show that *PNPLA6* has a role in photoreceptor survival and identify phospholipid metabolism as a potential therapeutic target for some forms of blindness.

Results

Identification of PNPLA6 mutations in OMS. Our initial goal was to discover the causal genetic mutations for two sporadic cases (5,267 and 5,273) in two Canadian families and three affected siblings (166, 167 and 169), in a third OMS family from the Czech Republic (Fig. 1). Although most OMS cases seem to be sporadic, segregation patterns of the phenotype support the recessive mode of inheritance. We therefore hypothesized that we could identify the unknown causal gene by excluding all genomic variants, except

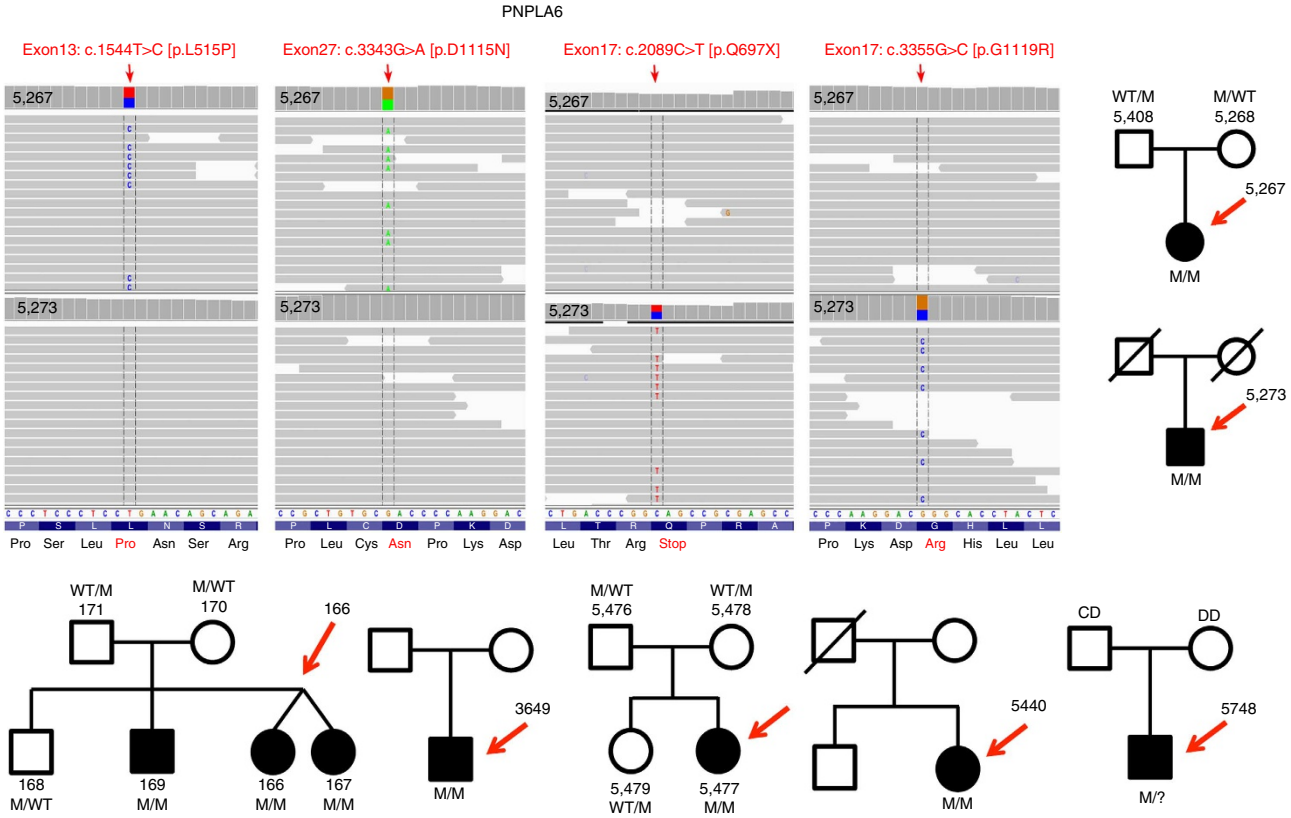

Figure 1 | *PNPLA6* mutations in individuals from seven families with childhood blindness. Sequencing reads are aligned against positive strand of hg19. Vertical arrows represent the 100 paired-end reads in 5,267 and 5,273 patients, respectively. Both patients carry heterozygous mutations in *PNPLA6*: 5,267 has 2 missense mutations c.1571T>C (leucine to proline substitution at codon 524) and c.3373G>A (aspartic acid to asparagine at codon 1125). Patient 5,273 has a nonsense mutation c.2116C>T, which result in a glutamine to stop codon at codon 706, leading to loss of the last 669 amino acids of the protein and a missense mutation c.3385G>C glycine to arginine at codon 1129. All of the complementary DNA positions are based on PNPLA6 NM_001166111.1. Moreover, shown are seven families/pedigrees with various forms of childhood blindness due to photoreceptor degeneration in OMS and LCA. Chromatograms of the *PNPLA6* mutations, pedigrees and co-segregation of the mutations are shown for each family (Supplementary Fig. 1).

those biallelic variants that we would find in the same gene in the five affected OMS patients (assuming one gene for OMS). Whole exome sequencing (WES) first excluded such mutations in the currently known 210 retinal disease genes. We then sifted through thousands of variants and identified that all five patients harboured and shared biallelic variants in *PNPLA6* and not in any other gene (Fig. 1). We identified six missense mutations in these three OMS families in *PNPLA6* (NM 001166111.1). With Sanger sequencing, we confirmed co-segregation in two out of the three families (one family was deceased) and excluded the variants from 100 normal controls. We then recruited five more OMS families from around the world (Fig. 1), and overall we identified ten novel *PNPLA6* mutations (Fig. 2b and Supplementary Fig. 1) in a total of seven families. Only one OMS family did not harbour *PNPLA6* mutations, suggesting allelic heterogeneity and thus a second OMS-causing gene. We then searched for *PNPLA6* mutations in 200 cases with LCA that had undergone WES and found one patient with significant autism and two *PNPLA6* mutations. We discovered a total of five missense, two nonsense, two frameshift and one splice site mutation(s) in *PNPLA6* (Figs 1 and 2). One of the mutations, that is, p. Gly1129Arg was found three times, while another mutation, that is, p. Asp1125Asn was identified twice, affecting residues in the evolutionarily highly conserved patatin domain (down to *Escherichia coli*; Fig. 2c). In five out of seven patients, we found compound heterozygous missense mutations in both the regulatory (amino-terminal) and in the catalytic domain (carboxy-terminal). The missense mutations are all in residues that are very well conserved (Fig. 2c). Targeted DNA screening revealed that the mutations found in the affected individuals are rare, as they were absent from >1,000 WES samples in our in-house databases of which at least 200 patients were genetically unsettled LCA.

Genotype/phenotype correlations in the cohort. All except one patient had OMS, as per standard clinical diagnostic criteria, with some patients exhibiting ataxia, mental retardation, or peripheral neuropathy. Detailed phenotypes are described in Table 1. All our OMS patients had significant retinal degeneration with photoreceptor death and blindness, long lashes and dwarfism. The retinal degeneration is severe and early onset, with photoreceptor death, but also with inner retinal changes and retinal thinning accompanied by lipofuscin metabolism abnormalities (Fig. 3).

In proband 5,267 from family 1, we found two missense mutations (Figs 1 and 2b and Supplementary Fig. 1) One of the missense mutations resides in a residue in the regulatory region and the second in the catalytic region (patatin domain) (Fig. 2). Briefly, this affected French–Canadian child with OMS developed nyctalopia (significant nightblindness) at the age of 2 years. At age 9 years, she had 20/1,200 visual acuities from severe retinal and choroidal degeneration (Fig. 3a), with diffuse photoreceptor loss (Fig. 3b), growth retardation and long lashes, but high intelligence. In proband 5,273 from family 2 with OMS, we found a nonsense mutation in the regulatory region and a missense mutation in the patatin domain of *PNPLA6* (Figs 1, 2b and Supplementary Fig. 1). This 30-year-old Scottish male had light perception vision photoreceptor loss, dwarfism, peripheral neuropathy and ataxia.

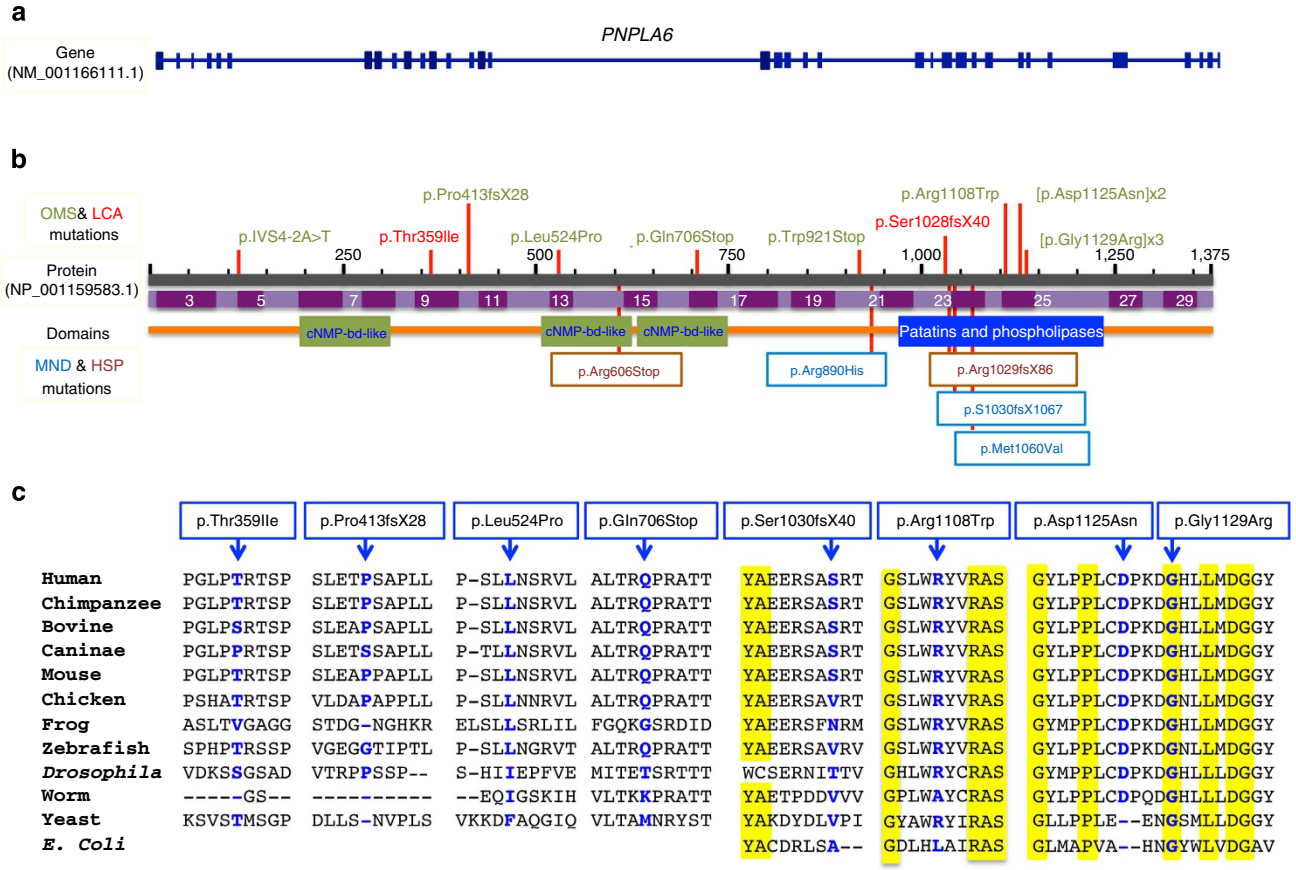

Figure 2 | Mutations identified in *PNPLA6* patients. Shown here is the genetic structure (**a**) and the protein structure (**b**) with all the mutations (ten) identified in the current study indicated above the PNPLA6 protein. Previously reported mutations causing the paraplegia syndrome (SPG39) are shown below the protein. A line-up of the affected protein regions from various species (from *E. coli* to man) is shown in **c**, showing the marked and significant evolutionary conservation of the residues, some down to *E. coli*.

In cases 166, 167 and 169 from the Czech OMS family 3 we found a splice site mutation in the regulatory region and a missense mutation in the patatin domain (Fig. 2b and Supplementary Fig. 1). The three affected members had severe photoreceptor degeneration, dwarfism, long lashes, normal intelligence, ataxia and peripheral neuropathy. Proband 3,649 from family 4 with LCA was found to have a frameshift in the catalytic region and a missense mutation in the regulatory region of *PNPLA6* (Fig. 2b and Supplementary Fig. 1). This Caucasian child had congenital visual loss and significant autism but no other systemic disease. Proband 5,477 from family 5 with OMS was found to have two missense mutations, both in the catalytic region, which co-segregate through this Brazilian family (Fig. 2b and Supplementary Fig. 1). The affected child has severe visual loss (counting fingers vision) from photoreceptor degeneration, long lashes, short stature, mild mental handicap and neuropathy with ataxia. Proband 5,440 from family 6 with OMS from Scotland carried a frameshift mutation in the regulatory region and a missense mutation in the catalytic region of *PNPLA6*, which co-segregated in the family (Fig. 2b and Supplementary Fig. 1). The affected child was noted to have congenital nystagmus from photoreceptor degeneration, normal mentation and lashes, but short stature and a motor neuropathy. Proband 5,748 from family 7 with OMS from Great Britain was found to harbour a nonsense mutation in the regulatory region of *PNPLA6*, shared by the father of the affected child, but we could not identify the maternal mutation (Fig. 2b and Supplementary Fig. 1).

PNPLA6 is expressed in mouse and fly photoreceptors. All our subjects with *PNPLA6* mutations have photoreceptor degeneration resulting in blindness. However, *PNPLA6* mutations associated with SPG39 and OPIDN diseases are not known to cause retinal degeneration or blindness. As it was previously not known whether *PNPLA6* is expressed in retinal tissue, we investigated the spatiotemporal retinal expression pattern of the PNPLA6 orthologues in *Drosophila* (SWS) and in mouse retina (Fig. 4a,b). Using an anti-serum against fly SWS, we found expression around photoreceptor nuclei and along the entire photoreceptor (Fig. 4c). Performing co-stainings with the plasma membrane marker anti-horseradish peroxidase, we found that some of the SWS is associated with the plasma membrane, but that it can also be found in the cytoplasm (Supplementary Fig. 2). This is in agreement with our previous results in central nervous system neurons, which showed that SWS can be detected in the ER[10]. In the mouse, we found PNPLA6-expressing cells in both developing and adult retinas (Fig. 4d–f). Co-staining of PNPLA6 with cell-type-specific

Table 1 | Complex phenotypes associated with *PNPLA6* mutations.

Patient MOGL study	5,267	5,273	166	167	169	3,649	5,477	5,440	5,748
Gender	F	M	F	F	M	M	F	F	M
Age at first exam (years)	9	29	3	3	16	0	2	2	0
Birth weight (kg)	2 kg	NA	3 kg	3.3 kg	1.9 kg	NA	2.5 kg	2.5 kg	2.4 kg
Height	Short	Short	Short	Short	Short	Normal	Short/ Dwarfism	Short	Short
Bone age	Delayed	NA	NA	NA	Normal	None	Delayed	Delayed	Delayed
Trichomegaly	Yes	Yes	Yes	Yes	Yes	No	NA	Normal	NA
Hair	Normal	Sparse	Alopecia	Normal	Alopecia	Normal	Alopecia	Alopecia	NA
Retinal degeneration	Yes	Yes	Yes	Yes	Yes	Yes	Yes	Yes	Yes
GH deficiency	Yes	Yes	Yes	Yes	Yes	None	Yes	Yes	Yes
Hypothyroidism	Yes	Yes	None	None	None	None	Yes	Yes	Yes
Hypogonadism	None	None	Yes	Yes	Yes	None	Yes	Yes	Yes
Mental retardation	None	None	None	None	None	Autism	Mild	None	Yes
Peripheral neuropathy and/or ataxia	None	Yes	Yes	Yes	Yes	None	Yes	Motor neuropathy	Yes
Inheritance	Sporadic	Sporadic	AR	AR	AR	Sporadic	NA	Sporadic	Sporadic
Chromosome	NA	46 XY	46 XX	46 XX	46 XY	NA	NA	46 XY	NA
Age when last seen (years)	9	30	22	22	31	20	23	54	20
VA	20/400 OD 20/400 OS	Light perception with projection in both eyes	NA	NA	NA	Counting fingers	Lower than 20/400	Light perception only	20/200 OD 20/80 OS
GVF	No measurable field	No measurable visual field	NA	NA	NA	No measurable field	No measurable field	No measurable field	Peripheral constriction
ERG	No recordable responses	No recordable responses	NA	NA	NA	NA	NA	No recordable responses	NA
Retinal appearance	Severe degeneration	Severe degeneration	Severe degeneration	Severe degeneration	Severe degeneration	Severe degeneration	Severe degeneration	Severe degeneration	Severe degeneration
Cancer	None	None	None	None	None	None	None	None	None
Dental history	None	Chalky white teeth, numerous cavities	tooth development abnormalities	tooth development abnormalities	tooth development abnormalities	None	None	Delay in dentition	None
Comments	None	None	Severe neonatal hyperbilirubinemia	Severe neonatal hyperbilirubinemia	Severe neonatal hyperbilirubinemia	Nystagmus	Retinal sparing around the optic disc. Optic disc normal appearance	Mild elevation of LFTs	Thoracic lumbar scoliosis

ERG, electroretinograms; F, female; GH, growth hormone; GVF, Goldmann visual field; LFT, liver function tests; M, male; NA, not available; OD, oculus dexter; OS, oculus sinister; VA, Snellen visual acuity.

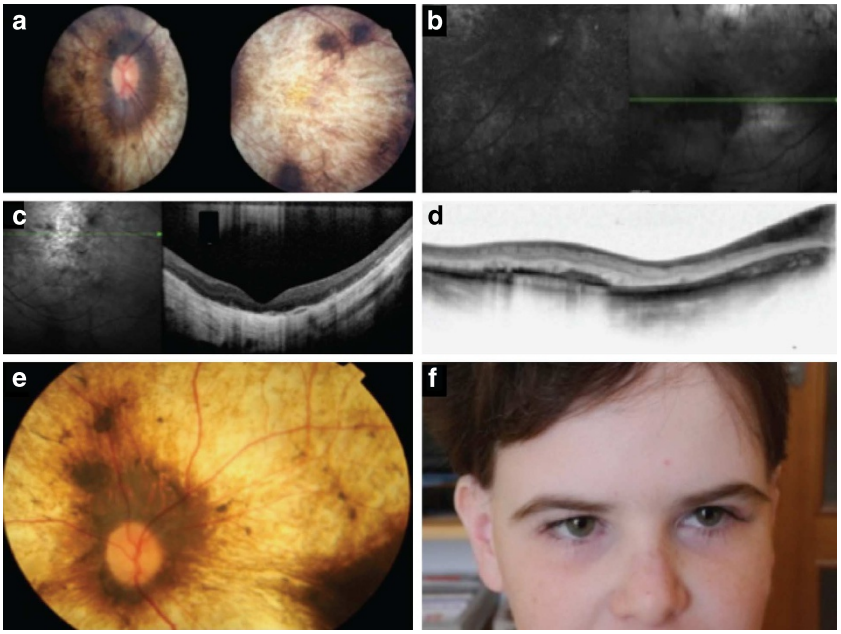

Figure 3 | Retinal phenotypes of children with *PNPLA6* mutations. (**a**) A retinal photo shows severe choroidal and retinal atrophy 'choroideremia like' in patient 5,267. (**b**) Fundus autofluorescence (FAF) shows severely abnormal and grossly absent lipofuscin metabolism. (**c**) Optical coherence tomography reveals severe photoreceptor loss, retinal thinning and retinal remodelling. (**d**) Using optical coherence tomography, we found that the inner retinal layers are also abnormal. (**e**) Another child (167) with mutations in *PNPLA6* shows a strikingly similar retinal appearance as shown in **a**, again illustrating the 'choroideremia-like' retinal changes. (**f**) Full-face photo of a child with *PNPLA6* mutations, illustrating the extremely long lashes.

markers showed restricted expression in horizontal, amacrine and photoreceptor cells (Fig. 4g–o), but not in ganglion cells (not shown). To determine the subcellular localization of PNPLA6 in photoreceptors, we co-stained adult mouse retinal sections with PNPLA6 and the inner segment (IS) plasma membrane marker Na^+/K^+ ATPase. Three-dimensional confocal imaging revealed clear co-labelling (Fig. 4p–r), indicating primarily IS plasma membrane localization in adult photoreceptors, although some intracellular staining was also observed (Fig. 4q). Interestingly, PNPLA6 was not found in the outer segments (OS). Peanut agglutinin co-staining in adult mice showed that PNPLA6 is also expressed in cones (Fig. 4s–u).

PNPLA6 is required for photoreceptor survival in *Drosophila*. To study the consequences of *PNPLA6* loss, we analysed the recessive *sws*^{1}-null mutant in *Drosophila*, which shows severe age-dependent neurodegeneration[15] starting around day five of adulthood, but no overt eye phenotype. Electron microscopic studies from *sws*^{1} flies shortly before eclosion revealed that the eye developed normally with all photoreceptors present (Fig. 5b). Whereas 14-day-old flies still had mostly intact ommatidia (occasionally one photoreceptor was lost, arrow, Fig. 5c), at 23 days the photoreceptors were either lost (arrows, Fig. 5d) or showed degenerative signs such as condensed cell bodies (arrowheads, Fig. 5d,f), intracellular membranous bodies (arrow, Fig. 5g), or vacuoles (arrowhead, Fig. 5h). Thirty-day-old wild-type flies did not reveal any of these phenotypes (Fig. 5a,e). To exclude that the photoreceptor degeneration is a secondary effect of the brain degeneration in *sws*^{1}, we also analysed an eye-specific knockdown of SWS using GMR-GAL4. Again, the photoreceptors developed normally (Fig. 5i,m) and still appeared unaffected in 7-day-old flies (Fig. 5j,n), but when 30 days old flies showed obvious signs of degeneration (Fig. 5k,o, arrows) and some photoreceptors were lost (Fig. 5k, arrowhead). To determine whether the degeneration was activity dependent, we raised the flies in the dark. As seen in Fig. 5l,p, this did not prevent the degeneration, showing that neuronal activity is not affecting the degeneration. To further assess a connection between degeneration and photoreceptor activity, we directly measured activity using electroretinograms (ERGs). Again, we could not detect any defects neither in young flies (1–3 days old) nor in aged ones (28–30 days old, Supplementary Fig. 3), which strongly suggests that phototransduction is not affected by the loss of SWS.

Mutations in *PNPLA6* alters phospholipid levels. Loss of SWS/PNPLA6 results in increased PC levels in flies and mice[10,13]. We therefore predicted that *sws*^{1} *Drosophila* as well as our OMS patients may show abnormalities in phospholipid levels due to lower PNPLA6 enzymatic activity. If true, this may then provide a tool for clinical diagnoses and potentially provide a therapeutic target. Based on the phospholipid metabolism showed in Fig. 6a, we predicted that mutant PNPLA6 (NTE) would result in elevated PC, LPC and LPA levels. This was confirmed using mass spectrometry analysis of these phospholipids in extracts from whole wild-type and mutant *Drosophila* (Fig. 6b). We also measured phospholipid levels in serum from family 1 (5,267) and family 3 (166–171) members. We found on average 10–15% increased levels of PC, LPA and LCA in patients and mutation carriers compared with controls (data not shown). However, as levels of these phospholipids are found to vary about two- to sixfold in normal human plasma/serum samples, with limited sample size and no opportunity to replicate these measurements in additional patients, the detected changes did not reach statistical significance.

Discussion

Our results suggest that *PNPLA6* is essential for vision and photoreceptor biology, and that mutations in *PNPLA6* cause photoreceptor neuron death and blindness in children with OMS

and LCA. Moreover, this report documents the first gene for OMS and the 20th gene for LCA. Finding *PNPLA6* mutations in various forms of childhood blindness was unexpected, because mutations and organophosphate-induced changes in PNPLA6 are observed in two neurological disorders with large motor neuron disease, spastic paraplegia (SPG39) and organophosphate-induced neuropathy (OPIDN). SPG39 and OPIDN are severe diseases but do not present with photoreceptor degeneration. Why do the mutations in *PNPLA6* described here cause photoreceptor cell death, while patients with SPG39 and OPIDN do not? One explanation is that the PNPLA6 mutations in five out of seven of our families were compound heterozygotes, with one mutation in the regulatory and one mutation in the catalytic domain (Fig. 2b and Supplementary Fig. 1). SPG39 patients have homozygous mutations in the catalytic (patatin) domain[12,16]. In OPIDN patients, the organophosphates bind to and inhibit only the catalytic domain and the N-terminal functions may not be affected. Having mutations in both domains may cause a more severe overall impairment of PNPLA6 function, leading to photoreceptor death. Alternatively, the mutations in the N-terminal regulatory domain might induce specific phenotypes. It is also possible that the harmful effects of organophosphates are not strong enough to affect retinal photoreceptors but only large neurons, such as motor neurons. It will be possible to test this hypothesis in future experiments.

PNPLA6 has been known for over 45 years and despite intense investigations (600 + publications), its various functions have not been fully elucidated[13]. Previously, *PNPLA6* was found to be expressed in the brain, most prominently in large (motor) neurons, but not in the retinal tissue[2,17]. We now show (Fig. 4) that PNPLA6 is expressed in the developing and mature mouse retina in horizontal, amacrine and photoreceptors cells, and in *Drosophila* photoreceptors. Unlike mouse neurons, where PNPLA6 localizes to the ER[12,18], we show here that PNPLA6 is mostly localized to the IS plasma membrane of mouse photoreceptors, suggesting a possible role for PNPLA6 in the formation of distinct plasma membrane domains in the IS and in the OS, or in the development/renewal of OS disc membranes, which are essential for maintaining the integrity of the photoreceptors and vision[16,19,20]. Previous studies indeed support a role for PNPLA6 in membrane growth, as knockdowns of *Pnpla6* in zebrafish caused axonal truncation and abnormal branching in addition to small eyes[17]. Furthermore, it was proposed that altered membrane trafficking in neuronal-specific *Pnpla6* knockout mice causes axonal degeneration in spinal neurons[13].

Similar to vertebrates, SWS is expressed in photoreceptor cells in flies. Although the photoreceptors develop normally in mutants, the eye-specific knockdown of SWS shows severe photoreceptor degeneration when aged, revealing that SWS is crucial for photoreceptor maintenance but not development. In addition, the degeneration is not dependent on light input,

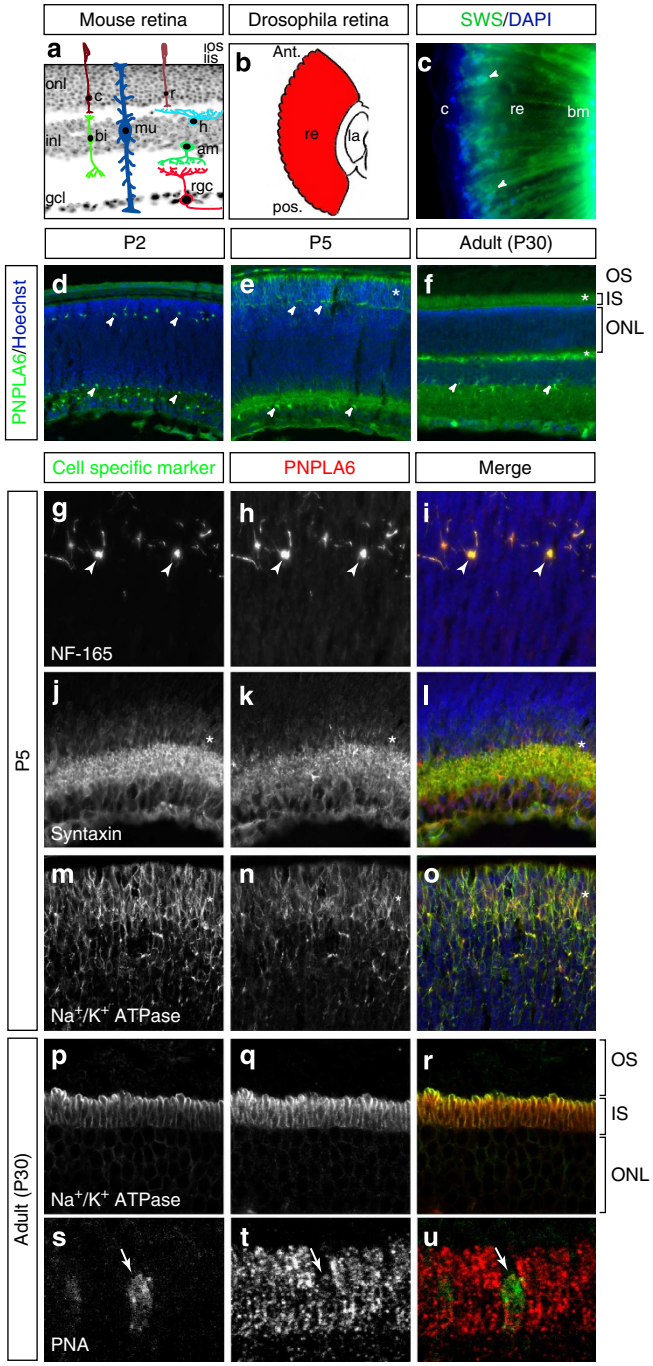

Figure 4 | PNPLA6 expression in the mouse and *Drosophila* retina. (**a**) Section of a mouse retina superimposed with illustrations of the cell types found in the three different layers. onl, outer nuclear layer; inl, inner nuclear layer; gcl, ganglion cell layer; os, outer segment; is, inner segment; r, rod; c, cone; mu, Müller cell; rgc, retinal ganglion cell; bi, bipolar cell; h, horizontal cell; am, amacrine cell. (**b**) Illustration of a *Drosophila* retina along the longitudinal axis. ant, anterior; pos, posterior; re, retina; la, lamina. (**c**) Immunostaining for SWS in longitudinal sections of fly retina. SWS is expressed surrounding the nuclei and along the entire length of the photoreceptor (arrowheads). bm, basement membrane; c, cornea; re, retina. (**d**–**f**) Time course of PNPLA6 expression in the mouse retina, as indicated. PNPLA6 is expressed in cells of the inner and outer retina at all stages examined (arrowheads), as well as in the photoreceptor inner segment area (asterisk). Co-immunostaining of mouse retinal sections at P5 with PNPLA6 and the horizontal cell marker neurofilament-165 (NF-165; **g**–**i**), amacrine cell marker syntaxin (**j**–**l**) and the photoreceptor cell marker Na^+/K^+-ATPase (**m**–**o**). Arrowheads point to positive cells and asterisks point to area of positive staining. (**p**–**r**) Confocal *z*-stack projection of an adult mouse retinal sections (P30) co-immunostained with PNPLA6 and the photoreceptor inner segment plasma membrane marker Na^+/K^+-ATPase. PNPLA6 localizes mostly to the plasma membrane, although some staining is detected inside the inner segment. (**s**–**u**) Co-immunostaining of PNPLA6 with the cone photoreceptor marker peanut agglutinin (PNA) showing expression of PNPLA6 in cones (arrow). Sections were counterstained with Hoechst (blue) to reveal nuclei.

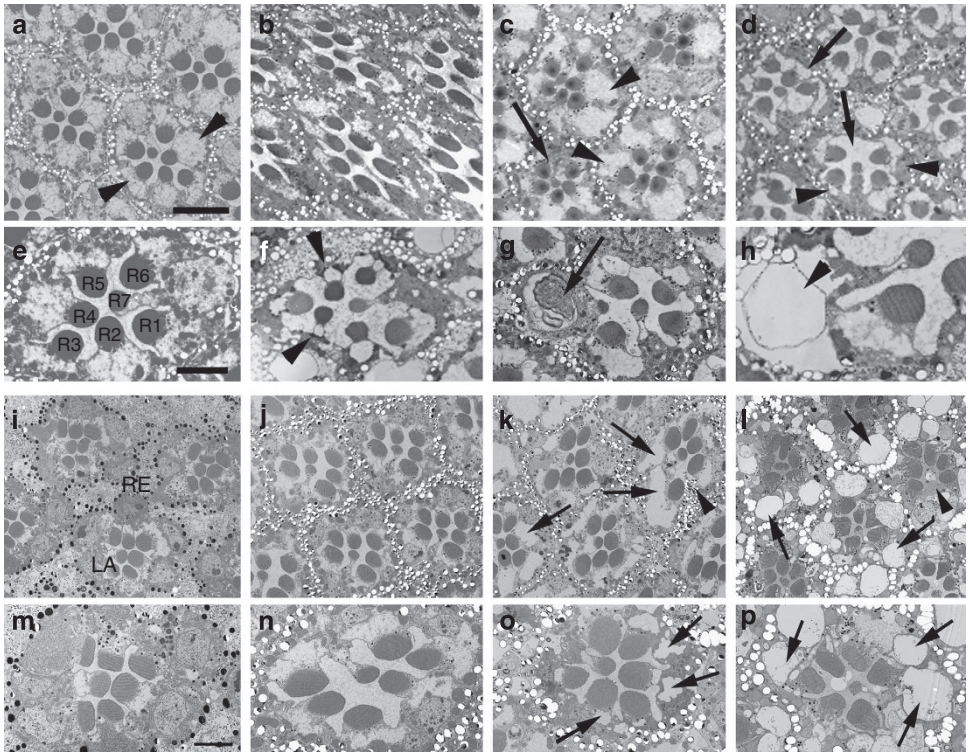

Figure 5 | Loss of SWS causes photoreceptor degeneration in *Drosophila*. Electron microscopy studies from a 3-week-old wild-type fly show intact ommatidia with seven photoreceptor cells (R1–7) present (**a**,**e**; arrowheads in **a** point to the photoreceptor cell somata). Performing sections from the retina of a *sws*^{1} mutant fly shortly before eclosion (pharate adult) shows that photoreceptors develop normally (**b**) and persist during the first 2 weeks of adulthood (**c**, 14 days), although occasionally ommatidia missing a single photoreceptor can be found (arrow). However, after 23 days of ageing (which, due to the reduced live span of *sws*^{1}, is shortly before these flies die), photoreceptor degeneration is evident in all ommatidia by the loss of photoreceptors (arrows in **d**), and in the condensed and darkly stained cell somata of the photoreceptors that are still present (arrowheads). In addition, vacuoles can be found in the somata (arrowheads in **f**,**h**) and the rhabdomeres are shrunken. In some photoreceptors, membranous structures can be found (arrow in **g**). Knocking down SWS specifically in the eye using an RNA interference (RNAi) construct expressed by GMR-GAL4 showed that newly enclosed flies look normal with all the seven photoreceptors R1–7 present (**i**,**m**). At 7 days of age the ommatidia still look wild type (**j**,**n**), but at 4 weeks the photoreceptors clearly show degeneration with vacuoles forming in the photoreceptor somata (arrows in **k**,**o**) and loss of some photoreceptors (arrowhead in **k**). Raising the flies in the dark resulted in a comparable photoreceptor degeneration in 30-day-old flies (**l**,**p**). Scale bar, 4 μm (**a**), 2 μm (**e**).

showing that the degeneration is not activity dependent. This suggests that the degeneration is caused by a failure to maintain the integrity of the photoreceptor cells and not by deleterious effects due to alterations in photoreception. This is also in agreement with the fact that the loss of SWS in other neurons also causes a progressive degeneration.

In agreement with the role of PNPLA6 as a phospholipase, we found alterations in phospholipid composition (LPC, LPA and PC) in *Drosophila*. We carefully examined the wild type, sws mutants and heterozygotes. Interestingly and importantly, we show a significant accumulation of all, LPA, LPC and LC, which may explain some of the clinical features of OMS. Indeed, elevated concentrations of LPA are known to be cytotoxic to neuronal cells, including photoreceptors[21], and defects in the LPC acyltransferase-1, an enzyme catalysing the conversion of LPC to PC, cause photoreceptor degeneration in mice[22]. LPA also promotes hair growth[23] and defects either in LPA production[24,25] or LPA signalling[26,27] are associated with hair growth abnormalities, as observed in our OMS patients. It is therefore possible that elevations in LPA lead to the trichomegaly, wooly hair and progressive alopecia in our OMS patients. Altered LPA signalling may also be responsible for the abnormalities in bone and tooth development[28], and growth hormone deficiency[25], also seen in our OMS patients (Table 1). Interestingly, transient juvenile trichomegaly and progressive alopecia, as well as a strong family history of different early-onset cancers[29] were also found in some of our families (data not shown). However, this link needs to be further explored.

Most of the identified mutations in OMS are in highly conserved residues, supporting their functional importance and potential use for rapid clinical testing of OMS and LCA patients. Our studies have opened a new avenue in investigating functions of *PNPLA6*, including whether single *PNPLA6* mutations increase photoreceptor susceptibility to environmental toxins. In the near future, it will be interesting to generate and characterize a photoreceptor-specific *Pnpla6* mouse knockout to study the fundamental mechanism of action of *PNPLA6* and evaluate the potential therapeutic benefits of lowering LPC and LPA.

Methods

Patient information. Patients were phenotyped at several international centres, after informed consents were obtained, approved by the ethical and scientific review boards. Detailed ophthalmological evaluations were followed by medical and clinical genetics consultations. All patients underwent a detailed history and pedigree analysis and detailed eye examinations, including best-corrected visual acuities by projected Snellen charts, near vision, slitlamp biomicroscopy and dilated retinal exams. *In vivo* retinal imaging was performed by the Heidelberg OCT (Heidelberg Engineering), followed by fundus autofluorescence. Kinetic fields were measured by Goldmann perimetry. In selected patients, we performed International Society for Clinical Electrophysiology of Vision (ISCEV) standard ERGs and multifocal ERGs (Diagnosys, Boston, USA). Peripheral blood was collected in lavender top (EDTA) tubes for DNA extraction.

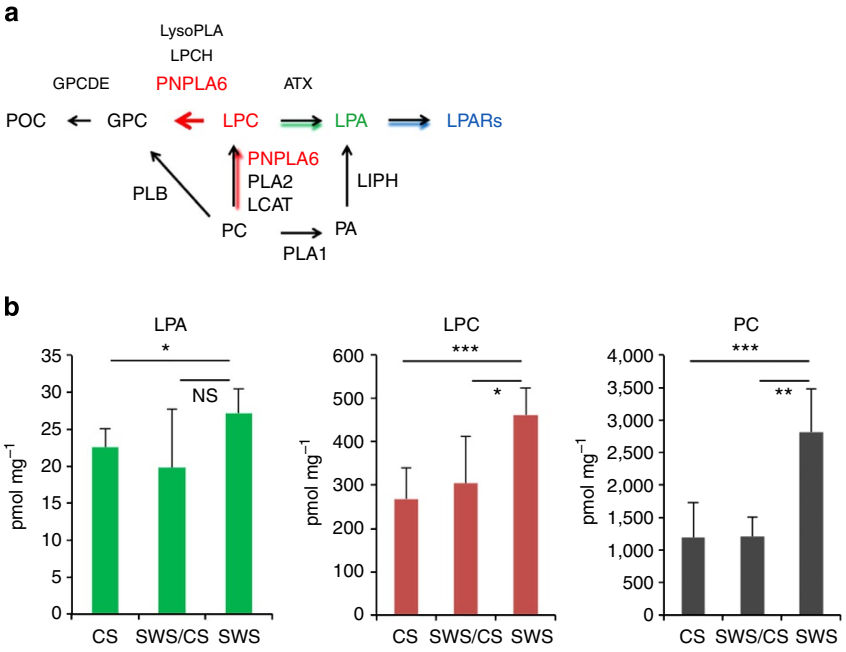

Figure 6 | Phospholipid metabolism is altered in SWS mutant flies. (**a**) PNPLA6 (NTE)-related metabolic pathway. POC, phosphorylcholine; GPC, glycerolphosphocholine; LPC, lysophosphatidylcholine; LPA, lysophosphatidic acid; LPARs, lysophosphatidic acid receptors; PCH, phosphatidylcholine; PA, phosphatidic acid; GPCDE, glycerolphosphocholinediesterase; NTE, neuropathy target esterase; LCAT, lecithin-cholesterol acyltransferase; PLA1, phospholipase A1; PLA2, phospholipase A1; PLB, phospholipase B; LPCH, lysophosphatidylcholine hydrolase; LIPH, lipase H; ATX, autotaxin. (**b**) Elevated PC, LPC and LPA levels in SWS mutant flies. Wild-type *Drosophila* (CS), ($n=8$); mutant heterozygotes (SWS/CS), $n=4$; *sws*^{1}-null mutants (SWS), $n=5$. PC, LPC and LPA levels (*y* axis) are expressed in pmol of individual compounds per mg of protein. The means ± s.d. for individual groups and *P*-values (*t*-test) are indicated; $^{*}P\leq0.05$, $^{**}P\leq0.01$, $^{***}P\leq0.001$; n.s., not significant. Experiments were repeated twice.

Animals. All animal work was carried out in accordance with the Canadian Council on Animal Care guidelines and was approved by the Institut de recherches cliniques de Montréal Animal Care Committee. CD1 and C57/Bl6 mice of either sex were used in this study.

WES analysis. DNA was extracted from whole blood using the FlexiGene kit or the QIAamp DNA blood kit according to the manufacturer's protocol. DNA quantity and quality were verified by using NanoDrop. The exomes of two sporadic cases (5,273 and 5,267) and all individuals from the Czech family 3 (166–171) with childhood blindness and OMS were captured by the Sure Select Human Exome Kit version 4 (Agilent Technologies, Inc., Santa Clara, CA), using 3 µg of genomic DNA of each. Exon-enriched DNA libraries were then sequenced either on Illumine HiSeq2000 that generate 100 bp paired-end reads or on SOLiD 4 that generate 50 bp reads. The details of bioinformatics analysis have been reported previously[30–33]. Briefly, the high-quality trimmed reads from Illumina HiSeq2000 were aligned to the positive strand of human genome (hg19) by BWA version 0.5.9 (ref. 29) and a mean coverage of 128 × (5,273) and 131 × (5,267) was obtained for the targeted coding regions (consensus coding sequence). Reads from SOLiD 4 were aligned using Novoalign version 2.08.03. Quality score recalibration was performed during alignment and reads that aligned to multiple locations were discarded. Following alignment PCR, duplicate reads were removed using Picard tools version 1.84. Variant calling and annotation were performed by SAMtools version 0.1.7 (ref. 34) and ANNOVAR[35], respectively. Filtering steps were carried out with public (dbsnp135, 1,000 genome project and NHLBI exomes) and our in-house exome (contains more than 800 samples) databases. Subsequently, variants that were predicted to be protein-altering (that is, missense, nonsense, frameshift, or canonical splice site changes) were prioritized and were manually examined in IGV[36]. Variants identified in individuals from Czech family 3 were also used for homozygosity mapping, linkage analysis and detection of copy-number variants.

Sanger sequencing and co-segregation. The selected variants were confirmed by Sanger sequencing in the patients and co-segregation was tested in their family members on an ABI 3730xl capillary sequencers. The Sanger sequencing results were analysed with the Sequencher software. Mutations were excluded from normal controls (at least 100 normal controls) and co-segregation in the family was studied. All mutations were studied by *in silico* analysis (Pmut, Blossum62, SIFT and Polyphen). All patients had two mutations, either homozygous or compound heterozygous. To ensure the completeness and quality of the sequences, primers were designed from intron sequences so that the entire exon and at least 50 bp of intron DNA on each side of each exon were amplified. Primers for the PCRs were designed by primer3 (http://frodo.wi.mit.edu/primer3/).

***Drosophila PNPLA6* localization and knockout experiments.** The 50-µm vibratome head sections from white-eyed flies (w^{1118}, to avoid interference by the autofluorescence from the eye pigment) were performed as described in Bolkan *et al.*[37] and stained with our anti-SWS serum at a dilution of 1:100. Detection was done with a biotinylated secondary antibody (1:200; Vector Laboratories) and a Cy5-conjugated streptavidin (1:100; Jackson ImmunoResearch). Sections were counterstained with DAPI (4′,6-diamidino-2-phenylindole; Invitrogen). Optical images (0.5 µm thick) were taken on an Olympus FW1000 confocal microscope. Semi-thin and ultra-thin Epon plastic sections were prepared as described in ref. 15. Semi-thin sections (1 µm) were stained with 1% toluidine blue and 1% borax, and analysed by light microscopy. Ultra-thin sections were analysed with a FEI Morgagni 268 electron microscope. *sws*^{1} is described in Kretzschmar *et al.*[15] ΔTM-SWS was created by deleting aa1–55, which includes the N terminus and the first transmembrane domain. The eye-specific knockdown was achieved by inducing the JF03428 RNA interference construct with GMR-GAL4 (both from the Bloomington Stock Center). Flies were raised and aged under standard conditions at 25 °C.

Mouse PNPLA6 immunostaining. Eyes were enucleated and fixed by immersion in freshly prepared 4% paraformaldehyde in PBS for 3 h on ice. For adult eyes, a small incision was made along the ora serrata after 10 min in paraformaldehyde, to allow better access to the fixative. The eyes were then rinsed in PBS and cryo-protected in sucrose 20% overnight, frozen and embedded in a sucrose:optimal cutting temperature (O.C.T.) compound (1:1) mix. For immunofluorescence, retinas were sectioned and processed for staining on the same day. Slides were preincubated for 1 h in blocking buffer (20% goat serum in 0.2% Triton) and then incubated 48 h at 4 °C with primary antibodies diluted in PBS. Primary antibodies used were PNPLA6 (NTE; 1/100, Abcam), $Na^{2+}K^{+}$-ATPase (1/100, Thermo Scientific), Syntaxin (1/500, Sigma), NF-165 (1/200, gift from B. Barres, Stanford U.) and Brn3b (1/100, Santa-Cruz). Bound antibodies were detected using appropriate secondary antibodies conjugated with Alexa 488, 555, 594 or 647 (1:1,000; Invitrogen) diluted in antibody buffer at room temperature for 1 h. In all cases, nuclei were counterstained with Hoechst 33342 (Molecular Probes).

Extraction of *Drosophila* phospholipids for flow injection-electrospray ionization-tandem mass spectrometry analysis. Whole flies were homogenized in MilliQ water to acquired concentration 80 mg ml^{-1}. Homogenization was performed with Branson Digital Sonifier 450 working as cup horn set to pulse mode (1 s pulse/1 s pause) with amplitude maximum at 100watt each sample was total homogenization time was 2 × 30 s. The 250 µl of fly homogenates was extracted by modified method of Natomi[38]. Fly homogenates (250 µl) corresponding to 20 mg was extracted by 2 ml of mixture of chloroform:methanol:water (20:10:1 v/v/v). Extraction mixture was repeatedly vortexed in 15-min steps during 2 h and then left at − 20 °C overnight. Supernatant was filtered through glass filter to a glass tube. Sediment was re-extracted with 2 ml of mixture of chloroform:methanol:water (10:10:1 v/v/v). Extraction mixture was vortexed for 1 h and then filtered through glass filter and combined with the first extract. Final re-extraction step was with 2 ml mixture of chloroform:methanol:water (10:20:1 v/v/v). The mixture was vortexed for 1 h and then filtered through glass filter and combined with previous extracts. The combined supernatants were dried under a stream of nitrogen. Aliquot corresponding to 1 mg of flies was mixed with 50 pmol of internal standards: C17:0 LPC, C17:0 LPA and C10:0PC (Avanti Polar Lipids Inc., Alabaster, Alabama, USA) and reconstituted in 1 ml of methanol with 5 mM NH_4COOH (to generate [M + H] + ions) or in pure methanol in the case of LPA (to generate [M-H]- ions). Samples were introduced by flow injection with tandem mass spectrometry (MS/MS).

Phospholipids analysis by FIA-ESI-MS/MS. Mass spectra were obtained on an ABI/MDS SCIEX API 4000 tandem mass spectrometer equipped with an electrospray ionization (ESI) source and coupled to an Agilent HPLC 1290 series.

PC and LPC were analysed by multiple reaction monitoring scans using common product ion with 184.1 *m/z* (phosphocholine) in the positive ion mode. Transition pairs were monitored for 100 ms and their *m/z* were as follows: LPC—494.3 → 184.1 (C16:1); 496.5 → 184.1 (C16:0); 520.4 → 184.1 (C18:2); 522.5 → 184.1 (C18:1); 524.5 → 184.1 (C18:0); 510.4 → 184.1 (C17:0 IST); PC: 732.6 → 184.1 (C32:3); 734.6 → 184.1 (C32:2); 742.6 → 184.1 (C33:3); 744.6 → 184.1 (C33:2); 746.6 → 184.1 (C33:1); 758.6 → 184.1 (C34:2); 760.6 → 184.1 (C34:1); 762.6 → 184.1 (C34:0); 780.6 → 184.1 (C36:3); 782.6 → 184.1 (C36:2); 784.6 → 184.1 (C36:1); 786.6 → 184.1 (C36:0); 794.7 → 184.1(C37:3); 796.7 → 184.1 (C37:2); 806.6 → 184.1 (C38:4); 808.6 → 184.1 (C38:3); 810.6 → 184.1 (C38:2); 812.7 → 184.1 (C38:1); 814.7 → 184.1 (C38:0); 426.6 → 184.1 (C10:0 IST). The ESI condition were as follows: curtain gas (N_2), 14 psi; collision gas (N_2), 7 psi; source gas 1 (N_2), 20 psi; source gas 2 (N_2), 50 psi; nebulizing gas (N_2) temperature, 200 °C; the capillary spray voltage was 5.5 kV, interface heater, ON. The ion optics settings for PC and LPC measurements were: 98 V for the declustering potential and 3 V for the entrance potential. The collision energy was set to 35 V, with a collision cell exit potential of 11 V. LPA was analysed by negative multiple reaction monitoring using 152.8 *m/z* product ion for LPA (glycerolphosphate): LPA 409.2 → 152.8 (C16:); 433.3 → 152.8 (C18:2); 435.4 → 152.8 (C18:1); 437.3 → 152.8 (C18:0); 457.2 → 152.8 (C20:4); 423.3 → 152.8 (C17:0 IST), and scan times for each transition pair was 500 ms. The ESI condition were as follows: curtain gas (N_2), 14 psi; collision gas (N_2), 12 psi; source gas 1 (N_2), 5 psi; source gas 2 (N_2), 25 psi; nebulizing gas (N_2) temperature, 200 °C; the capillary spray voltage was − 4.5 kV, interface heater, ON. The ion optics settings for LPA measurement were: − 118 V for the declustering potential and − 10.7 V for the entrance potential. The collision energy was set to − 35 V with a collision cell exit potential of − 5 V.

PC, LPC and LPA concentrations were calculated using known amount (50 pmol) of internal standard added to samples. Final concentrations were expressed as pmol of lipids per mg of *Drosophila*. The Analyst 1.5 software was used to operate the instruments and process the data.

References

1. Dudek, B. R. & Richardson, R. J. Evidence for the existence of neurotoxic esterase in neural and lymphatic tissue of the adult hen. *Biochem. Pharmacol.* **31,** 1117–1121 (1982).
2. Johnson, M. K. Initiation of organophosphate-induced delayed neuropathy. *Neurobehav. Toxicol. Teratol.* **4,** 759–765 (1982).
3. Glynn, P. Neuropathy target esterase and phospholipid deacylation. *Biochim. Biophys. Acta* **1736,** 87–93 2005.
4. Johnson, M. K. The delayed neurotoxic effect of some organophosphorus compounds. Identification of the phosphorylation site as an esterase. *Biochem. J.* **114,** 711–717 (1969).
5. Glynn, P. NTE: one target protein for different toxic syndromes with distinct mechanisms? *Bioessays* **25,** 742–745 (2003).
6. Hein, N. D., Rainier, S. R., Richardson, R. J. & Fink, J. K. Motor neuron disease due to neuropathy target esterase mutation: enzyme analysis of fibroblasts from human subjects yields insights into pathogenesis. *Toxicol. Lett.* **199,** 1–5 (2010).
7. Rainier, S. *et al.* Motor neuron disease due to neuropathy target esterase gene mutation: clinical features of the index families. *Muscle Nerve* **43,** 19–25 (2011).
8. Richardson, R. J., Hein, N. D., Wijeyesakere, S. J., Fink, J. K. & Makhaeva, G. F. Neuropathy target esterase (NTE): overview and future. *Chem. Biol. Interact.* **203,** 238–244 (2013).
9. Chang, P. A. & Wu, Y. J. Neuropathy target esterase: an essential enzyme for neural development and axonal maintenance. *Int. J. Biochem. Cell Biol.* **42,** 573–575 (2010).
10. Muhlig-Versen, M. *et al.* Loss of Swiss cheese/neuropathy target esterase activity causes disruption of phosphatidylcholine homeostasis and neuronal and glial death in adult *Drosophila*. *J. Neurosci.* **25,** 2865–2873 (2005).
11. Winrow, C. J. *et al.* Loss of neuropathy target esterase in mice links organophosphate exposure to hyperactivity. *Nat. Genet.* **33,** 477–485 (2003).
12. Akassoglou, K. *et al.* Brain-specific deletion of neuropathy target esterase/swisscheese results in neurodegeneration. *Proc. Natl Acad. Sci. USA* **101,** 5075–5080 (2004).
13. Read, D. J., Li, Y., Chao, M. V., Cavanagh, J. B. & Glynn, P. Neuropathy target esterase is required for adult vertebrate axon maintenance. *J. Neurosci.* **29,** 11594–11600 (2009).
14. Read, D. J., Li, Y., Chao, M. V., Cavanagh, J. B. & Glynn, P. Organophosphates induce distal axonal damage, but not brain oedema, by inactivating neuropathy target esterase. *Toxicol. Appl. Pharmacol.* **245,** 108–115 (2010).
15. Kretzschmar, D., Hasan, G., Sharma, S., Heisenberg, M. & Benzer, S. The swiss cheese mutant causes glial hyperwrapping and brain degeneration in *Drosophila*. *J. Neurosci.* **17,** 7425–7432 (1997).
16. Nilsson, S. E. Receptor cell outer segment development and ultrastructure of the disk membranes in the retina of the tadpole (*Rana pipiens*). *J. Ultrastruct. Res.* **11,** 581–602 (1964).
17. Song, Y. *et al.* Knockdown of Pnpla6 protein results in motor neuron defects in zebrafish. *Dis. Model. Mech.* **6,** 404–413 (2013).
18. Zaccheo, O., Dinsdale, D., Meacock, P. A. & Glynn, P. Neuropathy target esterase and its yeast homologue degrade phosphatidylcholine to glycerophosphocholine in living cells. *J. Biol. Chem.* **279,** 24024–24033 (2004).
19. Sahly, I. *et al.* Localization of Usher 1 proteins to the photoreceptor calyceal processes, which are absent from mice. *J. Cell Biol.* **199,** 381–399 (2012).
20. Anderson, D. H., Fisher, S. K. & Steinberg, R. H. Mammalian cones: disc shedding, phagocytosis, and renewal. *Invest. Ophthalmol. Vis. Sci.* **17,** 117–133 (1978).
21. Barth, C. & Stark, G. Radiation inactivation of ion channels formed by gramicidin A. Protection by lipid double bonds and by alpha-tocopherol. *Biochim. Biophys. Acta* **1066,** 54–58 (1991).
22. Friedman, J. S. *et al.* Loss of lysophosphatidylcholine acyltransferase 1 leads to photoreceptor degeneration in rd11 mice. *Proc. Natl Acad. Sci. USA* **107,** 15523–15528 (2010).
23. Takahashi, T., Kamimura, A., Hamazono-Matsuoka, T. & Honda, S. Phosphatidic acid has a potential to promote hair growth in vitro and in vivo, and activates mitogen-activated protein kinase/extracellular signal-regulated kinase kinase in hair epithelial cells. *J. Invest. Dermatol.* **121,** 448–456 (2003).
24. Kazantseva, A. *et al.* Human hair growth deficiency is linked to a genetic defect in the phospholipase gene LIPH. *Science* **314,** 982–985 (2006).
25. Rui, L., Archer, S. F., Argetsinger, L. S. & Carter-Su, C. Platelet-derived growth factor and lysophosphatidic acid inhibit growth hormone binding and signaling via a protein kinase C-dependent pathway. *J. Biol. Chem.* **275,** 2885–2892 (2000).
26. Pasternack, S. M. *et al.* G protein-coupled receptor P2Y5 and its ligand LPA are involved in maintenance of human hair growth. *Nat. Genet.* **40,** 329–334 (2008).
27. Shimomura, Y. *et al.* Disruption of P2RY5, an orphan G protein-coupled receptor, underlies autosomal recessive woolly hair. *Nat. Genet.* **40,** 335–339 (2008).
28. Blackburn, J. & Mansell, J. P. The emerging role of lysophosphatidic acid (LPA) in skeletal biology. *Bone* **50,** 756–762 (2012).
29. Li, H. & Durbin, R. Fast and accurate short read alignment with Burrows-Wheeler transform. *Bioinformatics* **25,** 1754–1760 (2009).
30. Fahiminiya, S. *et al.* Whole-exome sequencing reveals a heterozygous LRP5 mutation in a 6-year-old boy with vertebral compression fractures and low trabecular bone density. *Bone* **57,** 41–46 (2013).
31. Fahiminiya, S. *et al.* Mutations in WNT1 are a cause of osteogenesis imperfecta. *J. Med. Genet.* **50,** 345–348 (2013).
32. Hartmannova, H. *et al.* Isolated X-linked hypertrophic cardiomyopathy caused by a novel mutation of the four-and-a-half LIM domain 1 gene. *Circ. Cardiovasc. Genet.* **6,** 543–551 (2013).
33. Stranecky, V. *et al.* Mutations in ANTXR1 cause GAPO syndrome. *Am. J. Hum. Genet.* **92,** 792–799 (2013).
34. Li, H. *et al.* The sequence alignment/map format and SAMtools. *Bioinformatics* **25,** 2078–2079 (2009).
35. Wang, K., Li, M. & Hakonarson, H. ANNOVAR: functional annotation of genetic variants from high-throughput sequencing data. *Nucleic Acids Res.* **38,** e164 (2010).
36. Robinson, J. T. *et al.* Integrative genomics viewer. *Nat. Biotechnol.* **29,** 24–26 (2011).
37. Bolkan, B. J., Triphan, T. & Kretzschmar, D. Beta-secretase cleavage of the fly amyloid precursor protein is required for glial survival. *J. Neurosci.* **32,** 16181–16192 (2012).
38. Natomi, H., Sugano, K., Iwamori, M., Takaku, F. & Nagai, Y. Region-specific distribution of glycosphingolipids in the rabbit gastrointestinal tract: preferential enrichment of sulfoglycolipids in the mucosal regions exposed to acid. *Biochim. Biophys. Acta* **961,** 213–222 (1988).

Acknowledgements

We sincerely thank the children and parents involved in this study. We acknowledge the crucial support from the Foundation Fighting Blindness Canada (to I.M.M., M.C. and R.K.K.). Further funding came from the Canadian Institutes of Health Research (M.C. and R.K.K.) and NIH (EY022356-01, EY018571-05 and NS047663-09 to R.K.K., R.C. and D.K.). M.C. is a Senior Fellow of the Fonds de recherche du Québec-Santé/Fondation Antoine-Turmel. S.K. is supported by the Charles University institutional programmes PRVOUK-P24/LF1/3, UNCE 204011 and SVV2013/266504, and by BIOCEV—Biotechnology and Biomedicine Centre of the Academy of Sciences and Charles University (CZ.1.05/1.1.00/02.0109), from the European Regional Development Fund. Specific support was provided by grant NT13116-4/2012 and NT14015-3/2013 from the Ministry of Health of the Czech Republic. R.G. was supported by the Graduate School of Life Sciences (University of Wuerzburg). We gratefully acknowledge the indispensible work of Xia Wang, Hui Wang, Ms Eunice Esteban, Leah Wood MSc, Jonas Tapia RN and Renee Pigeon. We sincerely thank the Care4Rare Canada Steering Committee: Kym Boycott (leader; University of Ottawa), Jan Friedman (co-lead; University of British Columbia), Jacques Michaud (co-lead; Université de Montréal), Francois Bernier (University of Calgary), Michael Brudno (University of Toronto), Bridget Fernandez (Memorial University), Bartha Knoppers (McGill University), Mark Samuels (Université de Montréal) and Steve Scherer (University of Toronto). This work was funded in part by the Government of Canada through Genome Canada, the Canadian Institutes of Health Research and the Ontario Genomics Institute (OGI-049). Additional funding was provided by Genome Quebec, Genome British Columbia and the McLaughlin Centre. We thank Janet Marcadier (Clinical Coordinator) and Chandree Beaulieu (Project Manager) for their contribution to the infrastructure of the FORGE Canada Consortium. We acknowledge the contribution of the high-throughput sequencing platform of the McGill University and Génome Québec Innovation Centre, Montréal, Canada.

Author contributions

J.M. and S.F. designed, oversaw and interpreted the genome experiments. S.C., H.R., I.L., V.S., V.K., A.K., E.B. and D.S. performed the genetic studies. V.R. performed and interpreted immunohistochemical characterization in mouse retina. D.S. performed the fly genetic studies, and R.G. and C.H.F. performed the electroretinograms. V.S. and A.P. analysed exome-sequencing data, performed linkage analysis and provided bioinformatic support; H.H., K.H. and L.P. performed exome sequencing and mutation segregation studies; L.K. performed phospholipid analysis; A.B. was responsible for biosampling, clinical evaluation and genetic counselling of the Czech family. I.M.M., R.C., O.G.P.B., A.P., H.G., M.S., J.R.S., J.L.T., J.S., P.C., Care4Rare, E.B., R.G., C.H.F. and J.L.P. collected family data and provided DNA material. S.K., J.M., V.R., D.K., M.C. and R.K.K. interpreted results. D.K., M.C. and R.K.K. designed and oversaw the study. S.K., D.K., M.C. and R.K.K. wrote the manuscript, which was reviewed and approved by all co-authors.

Additional information

Accession codes: Sequence data has been deposited at the European Genome-phenome Archive (EGA, http://www.ebi.ac.uk/ega/), which is hosted by the EBI, under accession number EGAS00001001013.

Supplementary Information accompanies this paper at http://www.nature.com/naturecommunications

Competing financial interests: The authors declare no competing financial interests.

Reprints and permission information is available online at http://npg.nature.com/reprintsandpermissions/

How to cite this article: Kmoch, S. *et al.* Mutations in *PNPLA6* are linked to photoreceptor degeneration and various forms of childhood blindness. *Nat. Commun.* 6:5614 doi: 10.1038/ncomms6614 (2015).

The Care4Rare Canada Consortium

Kym Boycott[19], Alex MacKenzie[19], Michael Brudno[20], Dennis Bulman[19] & David Dyment[19]

[19]Children's Hospital of Eastern Ontario Research Institute, University of Ottawa, 401 Smyth Road, Ottawa, Ontario, Canada K1H 8L1. [20]Department of Computer Science, University of Toronto, 10 King's College Road, Toronto, Ontario, Canada M5S 3G4.